THE JOURNAL OF PHYSICAL CHEMISTRY B

ARTICLE

pubs.acs.org/JPCB

Numerical Solution of the Nonlinear Poisson−Boltzmann Equation for a Macroion Modeled as an Array of Non Overlapping Beads

Stuart A. Allison*

Department of Chemistry, Georgia State University, P.O. Box 4098, Atlanta, Georgia 30302-4098, United States

ABSTRACT: In this work, an approximate numerical procedure, AB, is developed to solve the nonlinear Poisson−Boltzmann equation around a macroion modeled as an array of non overlapping beads containing charges placed at their centers. The bead radii, their charges, and the relative bead configuration are arbitrary. In the limit of a single bead of arbitrary charge, the AB procedure is exact. For dimers and other bead arrays, it is possible to compare the approximate potentials derived using the AB procedure with exact potentials obtained by a boundary element, BE, procedure. Average surface or "zeta" potentials are examined for dimers, trimers, and tetramers. The bead size and charges are chosen to ensure that nonlinear charge effects are significant. In these test cases, the AB procedure is accurate to better than 5% over a wide range of ionic strength. Finally, the electrostatics of short duplex DNA (≤100 base pairs) are examined using both "smooth cylinder" and "touching bead" models. It is concluded that the modeling DNA as a string of touching beads using the AB procedure yields "zeta" potentials that are accurate to better than 10%.

1. INTRODUCTION

Electrostatic interactions of charged species in aqueous solution are of great importance in a wide range of chemical, biochemical, and colloidal systems. These include the pK_a of charge groups of peptides, proteins, and colloidal particles,[1−5] protein structure, stability, and function,[6] rates of diffusion controlled reactions,[7] and noncovalent association and binding equilibria.[8] Starting with the pioneering work of Debye and Huckel[9] and continuing to the present, the Poisson−Boltzmann, PB, equation has been successfully used in modeling a wide range of electrostatic interactions. For weakly charged systems, it is valid to approximate the PB equation with the linear PB, LPB, equation. For simple geometrical cases, this problem can be solved analytically.[9] (See also any standard text in physical, biophysical, or colloidal chemistry.) For a macroion modeled as a low dielectric "cavity" of arbitrary size, shape, and containing an arbitrary charge distribution within, numerical procedures beginning with the work of Warwicker and Watson[10] have been developed to numerically solve the LPB equation.

For highly charged species, it is necessary to go beyond the LPB and solve the nonlinear PB, NLPB, equation. It should be emphasized that the NLPB equation is not exact and has long been criticized on a number of grounds.[11,12] Renewed interest in the NLPB equation developed in the 1980s. A number of groups investigating the ionic distribution around high molecular mass duplex DNA have shown that the NLPB equation gives accurate electrostatic potentials and ion distributions for co- and counterions that are univalent and small as compared to the diameter of DNA.[13−15] This stimulated the development of numerical procedures to solve the NLPB equation around model macroions.[16−20] The most widespread procedures employ a discrete "Cartesian mesh" subdivision of space around the model macroion.[16,18,20] For capped and uncapped cylinder models of DNA, a non-Cartesian mesh procedure can be used[17] that is more convenient considering the geometry of the particle being modeled. Still more general is the boundary element, BE, procedure,[19] where the user has considerable freedom in designing a mesh that is tailor-made for the application at hand. Typically, the "innermost surface" is a series of interconnected triangular plates that conform to the actual surface of the macroion. The mesh then consists of a series of shells, not dissimilar to the layers of an onion, that increase in thickness as one moves away from the surface of the macroion.[21]

Even in the best of circumstances, these numerical procedures are time-consuming, and considerable effort has been devoted to finding the most efficient procedures possible.[18] A problem of considerable interest to us is calculating transport properties (such as electrophoretic mobilities) of large, highly charged, and flexible macroions modeled as arrays of non overlapping beads. These include peptides,[22] DNA,[23] and colloids such as latex particles[4] and metal oxides.[5] For flexible models of a peptide or DNA, it is necessary to generate many structures and average the potentials over the different conformations. In the present work, we develop an approximate, but rapid, procedure that solves the NLPB equation around a macroion that is modeled as an array of non overlapping beads. In the limit of a single bead, the procedure is exact. For a small number of touching beads, we are able to test our approximate procedure by comparing surface potentials with "exact" values derived from BE modeling.[19,21] The approximate procedure is correct to within 10% of exact

Received: February 16, 2011
Revised: March 9, 2011
Published: April 01, 2011

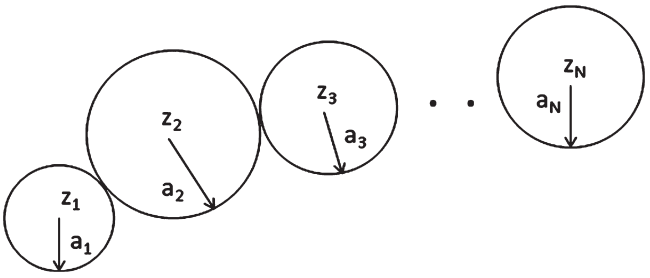

Figure 1. General bead array model. The model consists of N non overlapping beads. The valence charge and radius of bead j are z_j and a_j, where j varies from 1 to N. The bead radii, their charges, and there placement are arbitrary.

values for the cases considered in this work. In the Modeling section (section 2), we briefly review the BE procedure because it is used to test the "approximate bead", AB, procedure. To avoid a lengthy mathematical digression, which is probably of interest to only a limited audience, a detailed discussion of the AB procedure is placed in the Appendix. In section 3, we first compare BE and AB model results for dimers, trimers, and tetramers of touching bead models. This is followed by a modeling analysis of short duplex DNA (up to 100 base pairs). Here, we compare the "zeta" potential of short duplex DNA modeled as a right circular cylinder and also a bead array (both AB and more limited BE modeling). Section 4 concludes with a brief summar of the major findings of this work.

2. MODELING

The macroion is modeled as an array of N beads immersed in a medium of relative permittivity, ε_r, at temperature T. Let the valence charge and radius of bead j be z_j and a_j. The radii of the beads may vary, and the centroid position vector, $\underline{x}_j$, is arbitrary, but the beads cannot overlap. A schematic representation of our bead array is shown in Figure 1. Background electrolyte, BGE, is also present, and let $c_{\alpha 0}$ (in mol/L) and z_α denote the ambient concentration and valence of ionic species α. The nonlinear Poisson−Boltzmann equation, NLPB, can be written

$$\nabla^2\Psi(\underline{x}) = -\frac{\rho(\underline{x})}{\varepsilon_0\varepsilon_r} = -\frac{F}{\varepsilon_0\varepsilon_r}\sum_\alpha z_\alpha c_{\alpha 0} e^{-z_\alpha e\Psi(\underline{x})/k_B T} \quad (1)$$

Above, $\Psi(\underline{x})$ is the electrostatic potential at point $\underline{x}$, in the fluid, ∇^2 is the Laplacian operator, ρ is the local charge density, ε_0 is the permittivity of free space, F is the Faraday constant, e is the fundamental charge, and k_B is the Boltzmann constant. Equation 1 is solved subject to boundary conditions on the macroion surface that relates the charge within the macroion to the normal derivative of Ψ.[24]

For a spherical macroion containing a centrosymmetric charge distribution, eq 1 can be readily solved using long established numerical procedures.[25] For general model macroions, more complicated numerical procedures are available as discussed in the Introduction.[16−20] In the present work, the boundary element, BE, procedure[19,21,26] is used to numerically solve the NLPB equation around a single bead or bead array consisting of 2−4 touching beads of equal radii and equal charge placed at their centers. The surface of each bead is subdivided into 96−128 triangular plates. The fluid volume surrounding the bead array is subdivided into 50 shells increasing in thickness moving away from the bead surfaces, and each shell, in turn, is subdivided into a large number of volume elements.[21,26] The assumption is made that the electrostatic potential on each surface plate or within each volume element is constant. The accuracy of the assumptions can be tested for the case of a single bead using the simpler numerical procedure of ref 25. The BE results on dimers, trimers, and tetramers can then be used, in turn, to test the accuracy of the approximate bead, AB, model procedure.

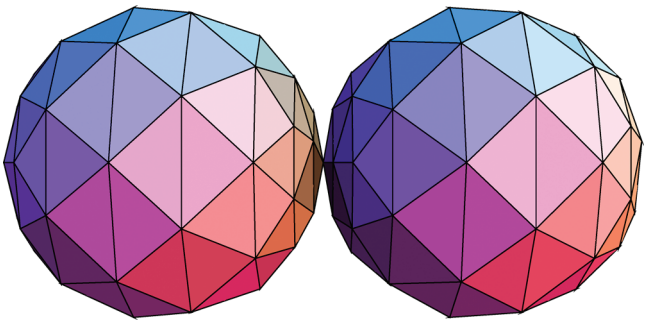

Figure 2. Boundary element model of a dimer of two touching monomers. Each monomer unit is represented as 112 triangular plates.

To avoid a lengthy mathematical digression, the detailed formulation of the AB procedure is placed in the Appendix. The Appendix also describes the assumptions made. Let ζ_j denote the average electrostatic surface potential of bead j and $\phi_j = e\zeta_j/k_B T$ denote the reduced (dimensionless) surface potential. These are obtained from eq A51, but an iterative procedure involving underrelaxation of results from previous iterations must be followed as discussed following eq A51 of the Appendix.

3. RESULTS

3.1. Comparison of Exact (BE) and Approximate (AB) Model Zeta Potentials of Monomers through Tetramer Bead Array Models. The radius of the basic monomer unit, a, shall be taken to be 1 nm with a valence charge of +10 placed at its center. This charge to radius ratio is quite large and insures that nonlinear contributions to the Poisson−Boltzmann equation are significant. The solvent is taken to be water plus added monovalent salt of ionic strength, I, in M = mol/L. The temperature, T, is set to 25 °C, solvent viscosity, η, is 0.089 poise, and relative permittivity, ε_r, is 78.54. For I = 0.03 M, a boundary element, BE, model sphere made up of 96−128 plates and hydrodynamic radius equal to 1 nm gives an average reduced surface or "zeta" potential, $\phi = e\zeta/k_B T = 3.85$. (Provided the surface is divided into more than 112 plates, the zeta potential is independent of the number of plates to a good approximation.) This is in excellent agreement with that obtained using the standard numerical procedure applied to a single spherical particle containing a centrosymmetric charge distribution.[25] On this basis, we conclude the BE results are "exact" and use them as a basis to test the approximate AB procedure on aggregates of the basic monomer unit. By hydrodynamic radius, R_h, we mean that the translational diffusion constant of the BE plate structure is identical to that of a smooth sphere of radius 1 nm. In what follows, the BE monomer unit is taken to be a 112 plate structure with R_h equal to 1 nm. Figure 2 shows the BE model of a touching dimer. The "contact" points are defined as the points on the sphere surfaces where the two spheres are closest to each other. More complex trimer and tetramer BE models are also considered in the present work.

The average reduced zeta potential, $\langle\phi\rangle_{BE}$, of a BE model at I = 0.03 M is +4.28 under conditions described in the previous

dx.doi.org/10.1021/jp201541g |J. Phys. Chem. B 2011, 115, 4872–4879

Table 1. Comparison of $\langle\phi\rangle$ for BE and AB Models of a Touching Dimer at Different Ionic Strengths

I (M)	κa	$\langle\phi\rangle_{BE}$	$\langle\phi\rangle_{AB}$	$1 - \langle\phi\rangle_{AB}/\langle\phi\rangle_{BE}$
0.001	0.1039	7.07	6.98	+0.013
0.003	0.1800	6.20	6.09	+0.018
0.010	0.3287	5.19	5.09	+0.019
0.030	0.5695	4.28	4.20	+0.019
0.100	1.0393	3.32	3.24	+0.024
0.300	1.800	2.47	2.41	+0.024

Table 2. Comparison of $\langle\phi\rangle$ for BE and AB Models of Bead Arrays at I = 0.03 M

N^a	geometry[b]	$\langle\phi\rangle_{BE}$	$\langle\phi\rangle_{AB}$	$1 - \langle\phi\rangle_{AB}/\langle\phi\rangle_{BE}$
1	single sphere	3.85	3.85	0.000
2	rod	4.28	4.20	0.019
3	rod	4.42	4.25	0.038
3	ring	4.49	4.39	0.022
4	rod	4.48	4.29	0.042
4	ring	4.58	4.43	0.033

[a] N = number of monomer unit. [b] A "rod" is an extended linear string of touching spheres, and a "ring" is a closed string of touching spheres.

paragraph. For a single isolated sphere or monomer, ϕ is uniform over the entire surface. However, the reduced potential on the surface of individual plates of the dimer ranges from +3.47 at the outermost ends to +7.78 for "contact" plates. In the dimer as well as higher aggregates, the reduced zeta potential varies considerably over the surface of an individual monomer unit, and this variation increases with increasing I. As discussed in the Appendix, an assumption of the AB procedure is that the reduced zeta potential at point $\underline{s}$ on the surface of a particular bead, j, $\phi_j(\underline{s})$, can be replaced with its average value, ϕ_j. An important question then is what effect does this assumption have on the accuracy of the potentials derived by the AB procedure. We can expect that the accuracy of the AB procedure deteriorates with increasing I, and we can test that hypothesis as well as the overall accuracy of the AB procedure by investigating the ionic strength dependence of $\langle\phi\rangle_{BE}$ and $\langle\phi\rangle_{AB}$ (the average reduced zeta potential obtained using the AB procedure) as a function of ionic strength. Table 1 summarizes $\langle\phi\rangle_{BE}$ and $\langle\phi\rangle_{AB}$ for touching dimer models over a wide range of I. The discrepancy between the approximate AB and exact BE results does increase with increasing I as expected, but the effect is gradual and even at the highest I considered, 0.30 M, is under 2.5%. Other conditions being equal, the discrepancy between $\langle\phi\rangle_{BE}$ and $\langle\phi\rangle_{AB}$ for a touching dimer of two beads of unequal radius decreases as the ratio of the bead radii deviates more strongly from unity. Despite variations in the potential over the surface of individual beads, the AB procedure is capable of predicting the average potential with considerable accuracy.

Table 2 compares the BE and AB models for short linear strings and also rings made up of N touching monomer units at I = 0.03 M. The discrepancy between the BE and AB models increases as N increases for rods, but the discrepancy appears to level off between N = 3 and 4. Also, the discrepancy is slightly larger for rods than rings (for constant N). This makes sense because we would expect the actual surface potential to show more variation for a rod relative to a ring for constant N. Even in the worst case in Table 2, however, the discrepancy is less than 5%. On that basis, we conclude that the AB model yields reduced zeta potentials that are accurate to about 5% or better.

3.2. Modeling the Zeta Potential of Short Duplex DNA. As mentioned in the Introduction, the major motivation of the present work concerns modeling flexible macromolecules such as peptides and DNA as non overlapping bead arrays.[21,22] Our ultimate goal is the determination of electrophoretic mobilities (and other electrokinetic transport properties) of these model structures, but determining equilibrium electrostatic potentials is a necessary first step in this endeavor. A key element in the parametrization of the bead radii of our "coarse grained" models is to find bead arrays that are able to reproduce the translational diffusion constant, D_t, of the actual structure. For peptides, each amino acid is modeled as two beads: a "backbone bead" of fixed radius (corresponding to one-half the average distance between the α carbons on nearest neighbor amino acids) and a "side bead" of variable radius.[27] The D_t of the specific amino acid is used to determine the side bead radius.[28] Duplex DNA has long been modeled as a wormlike chain of contour length, L, persistence length, P, and axial radius, R. The touching bead model initially developed by Hagermann and Zimm[29] captures many of the features of a continuous wormlike chain and continues to be used to the present day.[30] Although P for duplex DNA varies with ionic strength, it typically falls in the 50 nm size range.[31] Because the rise/base pair is 0.34 nm for duplex DNA, this corresponds to 147 base pairs, n_{bp}. For short DNA fragments (up to about n_{bp} equal to 100), we can model DNA as a right circular cylinder or linear string of touching beads. In the present work, we shall focus on this single special case to illustrate the bead array approach in a specific biophysical application.

The translational diffusion constant of a right circular cylinder of length L and axial radius R can be written:[32]

$$D_t = \frac{k_B T}{3\pi\eta L}(\ln(p) + \gamma(p)) \quad (2)$$

$$p = \frac{L}{2R} \quad (3)$$

$$\gamma(p) = 0.312 + 0.565/p + 0.100/p^2 \quad (4)$$

In eq 2, k_B is the Boltzmann constant, η is the solvent viscosity, and T is absolute temperature. The length is related to the number of base pairs simply by L (in nm) = $0.34 n_{bp}$. Also, R is 1.0 ± 0.1 nm,[33,34] and we shall set this to 1.0 nm. For short duplex DNA, eqs 2−4 can be used to determine D_t and this, in turn, can be used to determine the corresponding radius of our touching bead model, a. A particularly simple approach is to set $L = 2aN$ (N is the number of touching beads in our linear string) and adjust a so that the volumes of the cylinder and bead models are equal, or $a = (3/2)^{1/2}R$.[29,30] This approach is based on some early work by Garcia de la Torre and Bloomfield.[35] It is possible to improve upon this simple model because translational diffusion constants of linear strings of beads are now available to considerable accuracy.[36] For a linear string of N touching beads, we can write:

$$D_t = \frac{k_B T}{6\pi\eta a N^{1/3}} X_T(N) \quad (5)$$

The physical significance of X_T is that it corresponds to the ratio of D_t of our bead array to that of a sphere of equal volume. For N = 2, 3, 4, 6, and 8, $X_T(N)$ = 0.907, 0.84, 0.78, 0.70, and 0.65, respectively.[36]

Table 3. Zeta Potential of Bead Models of Duplex DNA in I = 0.02 M Monovalent Salt at 20 °C

N	n_{bp}	$-z$	$-\langle\phi\rangle_{LPB}$	$-\langle\phi\rangle_{BE}$	$-\langle\phi\rangle_{AB}$	$-\langle\phi\rangle_{cyl}$
2	11.12	11.12	6.52	4.54	4.50	
3	17.47	11.65	7.64	4.81	4.68	
4	23.82	11.91	8.27	4.91	4.78	
6	36.53	12.18	8.96		4.88	
8	49.24	12.31	9.30		4.92	
10	61.94	12.39	9.52		4.95	
16	100.06	12.51	9.84		4.99	
cylinder	20					4.95
cylinder	40					5.18
cylinder	60					5.29
cylinder	80					5.31
cylinder	100					5.32

Equating eqs 2 and 5 followed by rearrangement:

$$\frac{L}{a} = \frac{2N^{1/3}(\ln(p) + \gamma(p))}{X_T(N)} \quad (6)$$

Also set

$$L = 2a(N - c) = 0.34n_{bp} \quad (7)$$

In addition, the valence charge per base pair of DNA is −2, and so the valence charge per bead, z, is

$$z = -11.765a\left(1 - \frac{c}{N}\right) \quad (8)$$

The unknowns in the above three equations are the bead radius, a, and c, which can be viewed as an empirical constant. It is straightforward to construct an Excel spreadsheet in which a and c are defined as input parameters, and then the left and right-hand sides of eq 6 are computed for different N values. In the fitting procedure, we start by setting c equal to 0 and then vary a until the sum of the square of the differences between the left and right-hand sides of eq 6, SR, is minimized. Next, c is incremented by a small amount, and the procedure is repeated. Repeated application leads to that combination of a and c that minimizes SR overall. To a good approximation, this is given by c = 0.25 and a = 1.08 nm (with R = 1.0 nm). These parameters are used in eqs 6−8 to construct model bead arrays of short duplex DNA.

Table 3 summarizes our modeling of short duplex DNA. The temperature is taken to be 20 °C in a monovalent salt with I = 0.02 M. The first seven rows contain bead modeling results using eqs 7 and 8 with a = 1.08 nm and c = 0.25. To appreciate the significance of nonlinear charge effects in this system, the reduced potential derived using the linear PB equation is presented in the fourth column, $\langle\phi\rangle_{LPB}$. Full BE results on the bead arrays, where each monomer is represented with 112 plates, are presented in the fifth column, $\langle\phi\rangle_{BE}$. This is only included for N = 2, 3, and 4. Approximate AB reduced potentials are presented in the sixth column, $\langle\phi\rangle_{AB}$. Comparing $\langle\phi\rangle_{BE}$ and $\langle\phi\rangle_{AB}$, it is observed that the approximate potentials are lower than "exact" values, but only by a few percent at most. This is consistent with the observations of section 3.1.

A final issue we would like to address is how well do zeta potentials for DNA modeled as bead arrays compare to those of DNA modeled as a smooth cylinder. For short DNA cylinders under conditions identical to those of the bead arrays just considered, zeta potentials are available.[37] These come from BE studies that are similar in many respects to the BE modeling of the present work except that the surface structures are very different in the two cases. The final five rows in Table 3 give reduced zeta potentials, $\langle\phi\rangle_{cyl}$, for duplex DNA (I = 0.02 M, T = 20 °C) modeled as smooth cylinders 20−100 base pairs in length. The absolute potentials of the smooth cylinder model exceed $|\langle\phi\rangle_{AB}|$ by about 6%. Some of this discrepancy is due to approximations inherent in the AB procedure, but some is also due to differences in the surface model as well. We can conclude by saying that using a bead model and the AB procedure to calculate electrostatic potentials at the level of the nonlinear PB equation yields surface (zeta) potentials that are accurate to within 10%.

4. SUMMARY

An approximate procedure, AB, has been developed to estimate the electrostatic potential around a macroion by numerically solving the nonlinear Poisson−Boltzmann equation. The model is "coarse grained" in the sense that the fluid and ion atmosphere exterior to the macroion is modeled as a dielectric continuum, and the macroion itself is modeled as an array of non overlapping beads. For dimers, trimers, and tetramers, we are able to test the accuracy of the AB procedure by comparing average "zeta" potentials with "exact" values obtained from boundary element, BE, modeling. (The quotes around "exact" in the previous sentence are there to emphasize that solutions of the nonlinear Poisson−Boltzmann equation are, in themselves, approximate.) Zeta potentials derived by the AB procedure always fall below "exact" values by less than 5%. The electrostatic potential around short duplex DNA fragments (less than or equal to 100 base pairs) is examined to illustrate the usefulness and potential accuracy of the AB procedure. In this case, electrostatic potentials are determined to an accuracy of about 10%. Some of the discrepancy is due to approximations inherent in the AB procedure, but some is also due to representing duplex DNA as an array of touching beads. It should also be mentioned that the AB procedure is computationally fast. The CPU time to determine the fully converged average zeta potential around a 100 base pair duplex DNA fragment (modeled as 16 beads) requires less than 1 min of CPU time on a single processor of a Unix-based Silicon Graphics computer. The corresponding BE calculation on a smooth cylinder model is roughly 100 times longer.

In future work, we shall use the AB procedure in modeling the electrokinetic transport of macroions modeled as bead arrays. In the past, we have used "coarse grained" bead models to examine the electrophoretic mobility of weakly charged peptides.[22,27] The AB procedure will allow us to extend these studies to highly charged peptides as well as other highly charged macroions such as DNA. Although the applications in this work have been restricted to rigid bead arrays, the AB procedure should provide a way of modeling, in an approximate way, the electrostatics around flexible macromolecules as well. The situation is analogous to using ensembles of "frozen" wormlike chains to model the rotational dynamics of (flexible) duplex DNA restriction fragments.[29,38]

■ APPENDIX

The starting point of the boundary element, BE, method as applied to electrostatics is Green's second identity:

$$\int_V (f\nabla^2\Psi - \Psi\nabla^2 f)\, dV = \int_S (f\,\underline{\nabla}\,\Psi - \Psi\,\underline{\nabla} f)\cdot \underline{n}'\, dS \quad (A1)$$

where Ψ is the electrostatic potential we want to determine, f is some arbitrary trial function, and V denotes a volume of integration

dx.doi.org/10.1021/jp201541g |J. Phys. Chem. B 2011, 115, 4872–4879

bounded by an arbitrary surface or surfaces. The application of the BE method to the electrostatics of a single, irregularly shaped surface has been discussed in detail elsewhere.[19,26] Here, we are interested in applying the methodology to a bead array made up of N beads as shown in Figure 1. Let the valence charge and radius of bead j be z_j and a_j. The radii of the beads may vary, and their centroid position vectors, $\underline{x}_j$, are arbitrary. We shall, however, restrict our modeling to non overlapping beads. The bead array is immersed in a solvent of relative permittivity, ε_r, and temperature, T. Salt is also present, and let $c_{\alpha 0}$ (in mol/L) and z_α denote the ambient concentration and valence of species α.

For f in eq A1, we choose

$$f(\underline{x}, \underline{s}) = \frac{e^{-\kappa r}}{4\pi r} \tag{A2}$$

$$r = |\underline{x} - \underline{s}| \tag{A3}$$

$$\kappa = F\sqrt{\frac{2I}{\varepsilon_0 \varepsilon_r RT}} = 5.028\times 10^{11}\sqrt{\frac{I}{\varepsilon_r T}} \tag{A4}$$

$$I = \frac{1}{2}\sum_\alpha c_{\alpha 0} z_\alpha^2 \tag{A5}$$

In eqs A2−A5 above, $\underline{x}$ and $\underline{s}$are position vectors, κ is the Debye−Huckel screening parameter (in units of 1/m), I is the ionic strength (in mol/L), F is the Faraday constant, ε_o is the permittivity of free space, and R is the gas constant. The trial function defined by eq A2 has the property:

$$\nabla^2 f(\underline{x}, \underline{s}) = \kappa^2 f(\underline{x}, \underline{s}) - \delta(\underline{x} - \underline{s}) \tag{A6}$$

Above, ∇^2 acts on $\underline{x}$ but not $\underline{s}$, and δ is the Dirac delta function. In the fluid domain lying exterior to the beads, the electrostatic potential,Ψ, is assumed to obey the nonlinear Poisson−Boltzmann, NLPB, equation defined by eq 1 in the text.

Choose the volume of integration in eq A1 to be the fluid domain exterior to the bead array, V_e. Assume the electrostatic potential on the surface of bead j is constant, ζ_j. Equation A1 can then be written:

$$\begin{aligned}\Psi(\underline{s})\Phi(\underline{s}, V_e) = &-\int_{V_e} f(\underline{x}, \underline{s}) h(\underline{x})\, dV_x \\ &- \sum_{k=1}^{N}\int_{S_k} f(\underline{x}, \underline{s})\, \underline{\nabla}\Psi(\underline{x})\cdot \underline{n}(\underline{x})\, dS_x \\ &+ \sum_{k=1}^{N} \zeta_k \int_{S_k} \underline{\nabla} f(\underline{x}, \underline{s})\cdot \underline{n}(\underline{x})\, dS_x\end{aligned} \tag{A7}$$

$$\Phi(\underline{s}, V_e) = \left\{\begin{array}{ll} 1 & \text{if } \underline{s} \text{ lies in } V_e \\ 1/2 & \text{if } \underline{s} \text{ lies on a bead surface, } S_k \\ 0 & \text{if } \underline{s} \text{ lies inside a bead}\end{array}\right\} \tag{A8}$$

$$h(\underline{x}) = \nabla^2\Psi(\underline{x}) - \kappa^2\Psi(\underline{x}) \tag{A9}$$

In eq A7, $\underline{n}(\underline{x})$is the local outward normal (into the fluid) at point $\underline{x}$ on the surface of a particular bead. On the surface of bead j, we also have the electrostatic boundary condition:

$$\varepsilon_r \underline{\nabla}\Psi(\underline{x})\cdot \underline{n}(\underline{x}) = -\frac{\sigma(\underline{x})}{\varepsilon_0} \cong -\frac{ez_j}{4\pi\varepsilon_0 a_j^2} \tag{A10}$$

The last set of surface integrals in eq A7 can be dealt with in the following way. Suppose we had a constant potential, ζ_k, everywhere in space. Because Ψ is constant, all derivatives vanish. Also suppose we have a single bounding bead surface, S_k, and let V_{ek} denote the volume exterior to bead k. Equation A7 then reduces to

$$\zeta_k\Phi(\underline{s}, V_{ek}) = \kappa^2\zeta_k G_k(\underline{s}) + \zeta_k\int_{S_k} \underline{\nabla} f(\underline{x}, \underline{s})\cdot \underline{n}(\underline{x})\, dS_x \tag{A11}$$

$$\begin{aligned}G_k(\underline{s}) &= \int_{V_{ek}} f(\underline{x}, \underline{s})\, dV_x \\ &= \int_{a_k}^{\infty} x^2\, dx \int d\Omega_x \frac{e^{-\kappa|\underline{x} - \underline{s}|}}{4\pi|\underline{x} - \underline{s}|}\end{aligned} \tag{A12}$$

In eq A12, $d\Omega_x$ denotes the angular coordinates of $\underline{x}$. Using eqs A10 and A11 in eq A7:

$$\begin{aligned}\Psi(\underline{s})\Phi(\underline{s}, V_e) = &-\int_{V_e} f(\underline{x}, \underline{s}) h(\underline{x})\, dV_x \\ &+ \frac{e}{4\pi\varepsilon_0}\sum_{k=1}^{N}\frac{z_k}{a_k^2}\int_{S_k} f(\underline{x}, \underline{s})\, dS_x \\ &+ \sum_{k=1}^{N}\zeta_k[\Phi(\underline{s}, V_{ek}) - \kappa^2 G_k(\underline{s})]\end{aligned} \tag{A13}$$

To proceed, the following identity is useful:[39]

$$f(\underline{x}, \underline{s}) = \kappa\sum_{n=0}^{\infty}\sum_{m=-n}^{n} i_n(\kappa r_<) k_n(\kappa r_>) Y_{n,m}^*(\Omega_x) Y_{n,m}(\Omega_s) \tag{A14}$$

where i_n and k_n are modified spherical Bessel functions, $r_<$ ($r_>$) is the lesser (greater) of $|\underline{x}|$or $|\underline{s}|$, $Y_{n,m}$ is a spherical harmonic, * denotes complex conjugation, and Ω_x and Ω_s denote the angular coordinates of $\underline{x}$ and $\underline{s}$ in some convenient frame of reference. The lowest order modified spherical Bessel functions are $i_0(z) = \sinh(z)/z$ and $k_0(z) = e^{-z}/z$. From eq A2, we also have

$$f(\underline{x}, \underline{s}) = \frac{\kappa}{4\pi} k_0(\kappa|\underline{x} - \underline{s}|) \tag{A15}$$

Combining eqs A14 and A15:

$$\begin{aligned}&k_0(\kappa|\underline{x} - \underline{s}|) \\ &\quad = 4\pi\sum_{n=0}^{\infty}\sum_{m=-n}^{n} i_n(\kappa r_<) k_n(\kappa r_>) Y_{n,m}^*(\Omega_x) Y_{n,m}(\Omega_s)\end{aligned} \tag{A16}$$

Using eq A14, it follows that

$$\int_{S_k} f(\underline{x}, \underline{s})\, dS_x = \kappa a_k^2 i_0(\kappa r_{k<}) k_0(\kappa r_{k>}) \tag{A17}$$

where $r_{k<}$ ($r_{k>}$) is the lesser (greater) of a_k and $r_k \equiv |\underline{s} - \underline{x}_k|$. Using eq A14 in eq A12, it can be shown:

$$G_k(\underline{s}) = \left\{\begin{array}{ll} i_0(\kappa r_k) e^{-\kappa a_k}(1 + \kappa a_k)/\kappa^2 & r_k \le a_k \\ \left(1 - \frac{1}{2} k_0(\kappa r_k) s(\kappa a_k)\right)/\kappa^2 & r_k \ge a_k\end{array}\right\} \tag{A18}$$

$$s(z) = e^z(z - 1) + e^{-z}(z + 1) \tag{A19}$$

dx.doi.org/10.1021/jp201541g |J. Phys. Chem. B 2011, 115, 4872–4879

At this point, introduce the following dimensionless quantities:

$$\phi(\underline{s}) = \frac{e\Psi(\underline{s})}{k_B T} \tag{A20}$$

$$\phi_k = \frac{e\zeta_k}{k_B T} \tag{A21}$$

$$g(\underline{x}) = \frac{eh(\underline{x})}{k_B T} = -\left(\sum_\alpha m_\alpha z_\alpha e^{-z_\alpha \phi(\underline{x})} + \phi(\underline{x})\right) \tag{A22}$$

$$m_\alpha = \frac{c_\alpha}{2I} \tag{A23}$$

$$\omega = \frac{\kappa e^2}{4\pi\varepsilon_0 \varepsilon_r k_B T} \tag{A24}$$

Multiplying eq A13 by e/k_BT and using the above identities:

$$\phi(\underline{s})\Phi(\underline{s}, V_e) - \sum_{k=1}^{N} \phi_k[\Phi(\underline{s}, V_{ek}) - \kappa^2 G_k(\underline{s})]$$

$$= -\kappa^2 \int_{V_e} f(\underline{x}, \underline{s}) g(\underline{x})\, dV_x + \omega \sum_{k=1}^{N} z_k i_0(\kappa r_{k<}) k_0(\kappa r_{k>}) \tag{A25}$$

Now, we shall restrict ourselves to a point in the fluid, $\underline{s}$, near the surface of particular bead, j, where eq A25 reduces to

$$\phi(\underline{s}) = -\kappa^2 \int_{V_e} f(\underline{x}, \underline{s}) g(\underline{x})\, dV_x + \frac{1}{2}\sum_{k=1}^{N} \phi_k s(\kappa a_k) k_0(\kappa r_k) + \omega \sum_{k=1}^{N} z_k i_0(\kappa a_k) k_0(\kappa r_k) \tag{A26}$$

Up to this point, the only assumptions made are that the electrostatic potential and its normal derivative at the surface of individual beads are uniform. (See discussion following eqs A8−A10.)

In the limit of a weakly charged bead array, the volume integral on the right-hand side of eq A26 vanishes. Because of charge neutrality, we can write

$$\sum_\alpha m_\alpha z_\alpha = 0 \tag{A27}$$

Expanding the exponential in eq A22, we can write

$$g(\underline{x}) = \sum_{p=2}^{\infty} e_p \phi(\underline{x})^p \tag{A28}$$

$$e_p = \sum_\alpha \frac{(-z_\alpha)^{p+1} m_\alpha}{p!} \tag{A29}$$

For a general electrolyte, the leading term in eq A28 is of order ϕ^2, and for a symmetric binary electrolyte, it is of order ϕ^3. In addition to the fact that $g(\underline{x}) \to 0$ in the limit of a weakly charged bead array, we also expect $g(\underline{x})$ to only be significant near the bead array surface due to the rapid decay of $\phi(\underline{x})$ as one moves away from the surface of the array. It will prove convenient to subdivide V_e into N volume elements, V_{ek}. A fluid point is defined to lie in V_{ek} if it lies closer to the centroid of bead k, $\underline{x_k}$, than that of any other bead. It is straightforward, both geometrically and numerically, to identify which V_{ek} a particular point in space falls into. This is shown schematically in Figure 3. Without loss of generality, we can write:

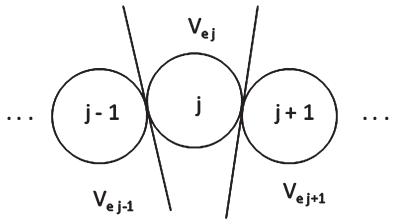

Figure 3. The subdivision of space external to the bead array. This is a two-dimensional rendition for the case of a string of touching beads where the plane of the paper passes through the center of the central bead, j, and its near neighbors ($j \pm 1$). The external volume, V_{ej}, lies closer to the center of bead j than to any other bead.

$$\kappa^2 \int_{V_e} f(\underline{x}, \underline{s}) g(\underline{x})\, dV_x = \sum_{k=1}^{N} H'_{kj}(\underline{s}) \tag{A30}$$

$$H'_{kj}(\underline{s}) = \kappa^2 \int_{V_{ek}} f(\underline{x}, \underline{s}) g(\underline{x})\, dV_x = \frac{\kappa^3}{4\pi} \int_{V_{ek}} k_0(\kappa|\underline{x} - \underline{s}|) g(\underline{x})\, dV_x \tag{A31}$$

Remember that we are considering a field point, $\underline{s}$, near bead j, and this accounts for the double subscript index on H'. Also, H'_{kj} is a dimensionless quantity. Equation A31 can also be written:

$$H'_{kj}(\underline{s}) = \frac{\kappa^3}{4\pi} \int_{a_k}^{\infty} x^2\, dx \int d\Omega_x\, k_0(\kappa|\underline{x} - \underline{s}|)\theta'_k(\underline{x}) g(\underline{x}) \tag{A32}$$

In eq A32, $\theta_k'(\underline{x})$ equals 1 if $\underline{x}$lies in V_{ek} and 0 otherwise.

At this point, three assumptions are made that greatly simplify the calculation of $H_{kj}'(\underline{s})$. In the limit of a single bead array carrying an arbitrary net charge, the assumptions become exact. The first assumption is that $\phi(\underline{x})$ in the domain V_{ek} is uniform for all points a distance $x = |\underline{x} - \underline{x_k}|$ from the center of bead k. This makes $g(\underline{x}) = g(x)$ in eq A32 (dependent only on the radial variable x). The second is to orientationally preaverage $k_0(\kappa|\underline{x} - \underline{s}|) = k_0(\kappa|(\underline{x} - \underline{x_k}) - (\underline{s} - \underline{x_j} - (\underline{x_k} - \underline{x_j}))|)$ over all $\underline{x}$ points a distance $x = |\underline{x} - \underline{x_k}|$ from the center of bead k and all $\underline{s}$ points a distance $s = |\underline{s} - \underline{x_j}|$ from the center of bead j. The third assumption shall be addressed in the next paragraph, but for now we shall focus on the case $k = j$, where eq A16 and the preaveraging approximation yields

$$k_0(\kappa|\underline{x} - \underline{s}|) \to i_0(\kappa r'_{j<}) k_0(\kappa r'_{j>}) \tag{A34}$$

Above, $r_{j<}'$ ($r_{j>}'$) is the lesser (greater) of $x = |\underline{x} - \underline{x_k}|$ and $s = |\underline{s} - \underline{x_j}|$. Using the first assumption above and eq A34 in eq A32 for the case $k = j$ yields:

$$H'_{jj}(\underline{s}) \approx k_0(\kappa s) H_{1j}(s) + i_0(\kappa s) H_{2j}(s) \tag{A35}$$

$$H_{1j}(s) = \kappa^3 \int_{a_j}^{s} x^2\, dx\, i_0(\kappa x)\theta_j(x) g_j(x) \tag{A36}$$

dx.doi.org/10.1021/jp201541g |J. Phys. Chem. B 2011, 115, 4872–4879

$$H_{2j}(s) = \kappa^3 \int_s^\infty x^2\, dx\, k_0(\kappa x)\theta_j(x)g_j(x) \quad \text{(A37)}$$

$$\theta_j(x) = \frac{1}{4\pi}\int d\Omega_x \theta_j'(\underline{x}) \quad \text{(A38)}$$

A subscript, j, has been added to $g(x)$ to emphasize that the quantity is being evaluated in the vicinity of bead j. The physical significance of $\theta_j(x)$ defined by eq A38 is that it represents the fraction of the spherical shell of radius $x = |\underline{x} - \underline{x_j}|$ centered on bead j and thickness dx that lies in V_{ek}. For the example of a linear string of beads where the neighboring beads of j are labeled $j-1$ and $j+1$, it is given by

$$\theta_j(x) = \frac{1}{2}(t(j-1) + t(j+1)) \quad \text{(A39)}$$

$$t(j \pm 1) = \left\{ \begin{array}{ll} 1 & x < x_{j,j\pm1}/2 \\ x_{j,j\pm1}/(2x) & x > x_{j,j\pm1}/2 \end{array} \right\} \quad \text{(A40)}$$

In eq A40, $x_{j,j\pm1} = |\underline{x_j} - \underline{x_{j\pm1}}|$. In the event bead j lies at the beginning ($j = 1$) or end ($j = N$) of the chain, then $t(0) = 1$ or $t(N+1) = 1$, respectively.

For the case $k \neq j$, we now make a third assumption and that is that $x = |\underline{x} - \underline{x_k}| < |\underline{s} - \underline{x_k}|$. In evaluating the volume integral defined by eq A32, this appears to be a reasonable assumption because $g(x)$ is expected to be greatest for $x \approx a_k$, yet the smallest x value is expected to be comparable to $x_{jk} = |\underline{x_{jk}}| = |\underline{x_j} - \underline{x_k}|$. Preaveraging over $\underline{x}$ (second assumption) gives

$$k_0(\kappa|\underline{x} - \underline{s}|) \rightarrow i_0(\kappa x)k_0(\kappa|(\underline{s} - \underline{x_j}) - \underline{x_{jk}}) \quad \text{(A41)}$$

The second assumption is invoked again (preaveraging over $\underline{s}$), and eq A41 becomes

$$k_0(\kappa|\underline{x} - \underline{s}|) \rightarrow i_0(\kappa x)i_0(\kappa r_{jk<})k_0(\kappa r_{jk>}) \quad \text{(A42)}$$

where $r_{jk<}$ ($r_{jk>}$) is the lesser (greater) of $s = |\underline{s} - \underline{x_j}|$ and x_{jk}. Using eqs A36−A38 and eq A42 along with the first assumption in eq A32 gives

$$H_{kj}'(\underline{s}) \approx i_0(\kappa r_{jk<})k_0(\kappa r_{jk>})H_{1k}(\infty) \quad \text{(A43)}$$

Equation A26 can now be put into a useful form for numerical purposes. We first average eq A26 over all $\underline{s}$ points a distance $s = |\underline{s} - \underline{x_j}|$ from the center of bead j to give $\phi_j(s)$. (In this notation, $\overline{\phi_j}$ is short for $\phi_j(a_j)$). Using eq A16 and averaging over Ω_s for $k_0(\kappa r_k)$ along with eqs A30−A32, A35, and A43:

$$\phi_j(s) = (d_j - H_{1j}(s))k_0(\kappa s) - H_{2j}(s)i_0(\kappa s) + \sum_{k\neq j=1}^{N} (d_k - H_{1k}(\infty))i_0(\kappa r_{jk<})k_0(\kappa r_{jk>}) \quad \text{(A44)}$$

$$d_k = \frac{1}{2}\phi_k s(\kappa a_k) + \omega z_k i_0(\kappa a_k) \quad \text{(A45)}$$

Equation A44 represents the master equation for determining the averaged reduced electrostatic potential a distance s from the center of bead j. Once the bead array (bead radii, their charges, and bead centroid coordinates) and solvent/buffer conditions are defined, all quantities in eqs A44 and A45 are known except for the ϕ_k, H_{1k}, and H_{2k} terms. Assume for the moment that we have estimates (from an initial assumption or previous iteration) of the H_{1k} and H_{2k} terms. In the limit $s \rightarrow a_j$, eq A44 reduces to

$$\sum_{k=1}^{N} A_{jk}\phi_k = \gamma_j \quad \text{(A46)}$$

$$A_{jk} = \left\{ \begin{array}{ll} 1 - \frac{1}{2}s(\kappa a_j)k_0(\kappa a_j) & j = k \\ -\frac{1}{2}s(\kappa a_k)i_0(\kappa a_j)k_0(\kappa x_{jk}) & j \neq k \end{array} \right\} \quad \text{(A47)}$$

$$\gamma_j = \gamma_j^0 - i_0(\kappa a_j)H_{2j}(a_j) - k_0(\kappa a_j)H_{1j}(a_j) - \sum_{k\neq j=1}^{N} i_0(\kappa a_j)k_0(\kappa x_{jk})H_{1k}(\infty) \quad \text{(A48)}$$

$$\gamma_j^0 = \omega z_j i_0(\kappa a_j)k_0(\kappa a_j) + \omega \sum_{k\neq j=1}^{N} z_k i_0(\kappa a_k)i_0(\kappa a_j)k_0(\kappa x_{jk}) \quad \text{(A49)}$$

The only unknowns in eq A46 are the ϕ_k terms. This can be put in matrix form (where $\underline{\underline{A}}$ is an N by N matrix and $\underline{\phi}$ and $\underline{\gamma}$ are N by 1 column vectors:

$$\underline{\underline{A}} \cdot \underline{\phi} = \underline{\gamma} \quad \text{(A50)}$$

The matrix $\underline{\underline{A}}$ is invertible, and let $\underline{\underline{A}}^{-1}$denote the inverse of $\underline{\underline{A}}$. Premultiplying both sides of eq A50 by $\underline{\underline{A}}^{-1}$yields

$$\underline{\phi} = \underline{\underline{A}}^{-1} \cdot \underline{\gamma} \quad \text{(A51)}$$

This gives us the reduced potentials on the bead surfaces (the ϕ_j terms).

As suggested previously, it is necessary to solve the problem iteratively because the potential, $\phi_j(s)$, in eq A44 appears implicitly on the right-hand side through the H_{1j} (eq A36) and H_{2j} (eq A37), and, within these, through $g(x)$ (eqs A22 and A28). As an initial estimate, it is assumed $g^{(1)}(x) = 0$, and from eqs A36 and A37, $H_{1j}{}^{(1)}$ and $H_{2j}{}^{(1)}$ vanish. (The superscript "(1)" is now being introduced to indicate the iteration number.) From eq A48, $\gamma_j{}^{(1)} = \gamma_j{}^0$, and from eq A49, these are known because the bead radii, charges, and coordinates are known along with the solvent/buffer conditions. From eq A51, we can now determine $\phi_j{}^{(1)}$. It should be emphasized that $\underline{\underline{A}}$ and $\underline{\underline{A}}^{-1}$only have to be determined once. After the $\phi_j{}^{(1)}$ values are determined, eq A44 can be used to determine $\phi_j{}^{(1)}(s)$ around each bead. For a weakly charged bead array, we can stop here because $g_j(x)$ is small and the H_{1j} and H_{2j} terms make little contribution to γ_j.

For highly charged bead arrays, however, further iterations are necessary. Starting with the second iteration ($n = 2$), we shall approximate $g_j^{(n)}(x)$ (see eq A28) with a finite sum of terms involving previous estimates of the potential $\phi_j^{(n-1)}(x)$:

$$g_j^{(n)}(x) = \sum_{p=2}^{p^*} e_p(\phi_j^{(n-1)}(x))^p \quad \text{(A52)}$$

where p^* is the maximum term in the finite sum. This is initially set to 3, and e_p is defined by eq A29. These are then used in

eqs A36 and A37 to numerically determine the integrals

$$H'^{(n)}_{1j}(s) = \kappa^3 \int_{a_j}^{s} x^2\, dx\, i_0(\kappa x)\theta_j(x) g_j^{(n)}(x) \quad \text{(A53)}$$

$$H'^{(n)}_{2j}(s) = \kappa^3 \int_{s_j}^{\infty} x^2\, dx\, k_0(\kappa x)\theta_j(x) g_j^{(n)}(x) \quad \text{(A54)}$$

It has been our experience that if eqs A53 and A54 are used directly to obtain updated estimates of H_{1j} and H_{2j}, the potentials diverge. Consequently, a procedure of "under relaxation"[16,17,26] is employed where we set (v = 1 or 2):

$$H_{vj}^{(n)}(s) = H_{vj}^{(n-1)}(s) + \lambda[H'^{(n)}_{vj}(s) - H'^{(n-1)}_{vj}(s)] \quad \text{(A55)}$$

In eq A55, λ represents the relaxation parameter that is usually set in the 0.10−0.25 range. If λ is set too high, the potentials diverge. If λ is set too low, convergence is slow.

Once the $H_{vj}^{(n)}(s)$ arrays have been computed starting with the second iteration (n = 2), eq A48 is used to determine $\gamma_j^{(2)}$, and then eq A51 is used to determine $\phi_j^{(2)}$. Finally, eq A44 is used to determine $\phi_j^{(2)}(s)$, and this completes the second iteration. To begin the third iteration, eq A52 is used to determine $g_j^{(3)}(x)$, and the whole procedure is repeated until the $\phi_j^{(n)}$ terms converge to within a predefined tolerance level. Once convergence is achieved, p^* (see eq A52) is raised by 2 (from 3 to 5, for example), and the iterative procedure is again continued until the $\phi_j^{(n)}$ terms converge as before. Next, p^* is again incremented by 2. This procedure is repeated until further increases in p^* have no further effect on the $\phi_j^{(n)}$ values. This is typically achieved for $p^* \approx 15$. At this point, it is assumed that overall convergence is achieved.

AUTHOR INFORMATION

Corresponding Author

*Phone: (404) 413-5519. E-mail: sallison@gsu.edu.

REFERENCES

(1) Yang, A.-S.; Gunner, M. R.; Sampogna, R.; Sharp, K.; Honig, B. *Proteins* **1993**, *15*, 252–265.
(2) Antosiewicz, J.; Briggs, J. M.; Elcock, A. H.; Gilson, M. K.; McCammon, J. A. *J. Comput. Chem.* **1996**, *17*, 1633–1644.
(3) Zhou, H.-X.; Vijayakumar, M. *J. Mol. Biol.* **1997**, *267*, 1002–1011.
(4) Allison, S. A.; Xin, Y. *J. Colloid Interface Sci.* **2006**, *299*, 977–988.
(5) Allison, S. A. *J. Colloid Interface Sci.* **2009**, *332*, 1–10.
(6) Nakamura, H. *Q. Rev. Biophys.* **1996**, *29*, 1–90.
(7) Davis, M. E.; Madura, J. D.; Sines, J.; Luty, B. A.; Allison, S. A.; McCammon, J. A. *Methods Enzymol.* **1991**, *202*, 473–498.
(8) Gilson, M. K.; Given, J. A.; Bush, B. L.; McCammon, J. A. *Biophys. J.* **1997**, *72*, 1047–1069.
(9) Debye, P.; Huckel, E. *Phys. Z.* **1923**, *24*, 185–206.
(10) Warwicker, J.; Watson, H. C. *J. Mol. Biol.* **1982**, *157*, 701–710.
(11) Fowler, R. H. *Statistical Mechanics*; Cambridge University Press: Cambridge, U.K., 1929.
(12) Onsager, L. *Chem. Rev.* **1933**, *13*, 73–89.
(13) Fixman, M. *J. Chem. Phys.* **1979**, *70*, 4995–5005.
(14) LeBret, M.; Zimm, B. H. *Biopolymers* **1984**, *23*, 270–285.
(15) Murthy, C. S.; Bacquet, R. J.; Rossky, P. J. *J. Phys. Chem.* **1985**, *89*, 701–710.
(16) Jayaram, B.; Sharp, K. A.; Honig, B. *Biopolymers* **1989**, *28*, 975–993.
(17) Allison, S. A. *J. Phys. Chem.* **1994**, *98*, 12091–12096.
(18) Holst, M. J.; Saied, F. *J. Comput. Chem.* **1995**, *16*, 337–364.
(19) Zhou, H.-X. *J. Chem. Phys.* **1994**, *100*, 3152–3162.
(20) Baker, N. A.; Sept, D.; Simpson, J.; Holst, M. J.; McCammon, J. A. *Proc. Natl. Acad. Sci. U.S.A.* **2001**, *98*, 10037–10041.
(21) Allison, S. A. *Biophys. Chem.* **2001**, *93*, 197–213.
(22) Pei, H.; Allison, S. A. *J. Chromatogr., A* **2009**, *1216*, 1908–1916.
(23) Allison, S. A.; Pei, H.; Xin, Y. *Biopolymers* **2007**, *87*, 102–114.
(24) Tanford, C. *Physical Chemistry of Macromolecules*; John Wiley and Sons: New York, 1961; Chapter 7.
(25) Loeb, A. L.; Overbeek, J.; Th., G.; Wiersema, P. H. *The Electrical Double Layer Around a Spherical Colloid Particle*; The M.I.T. Press: Cambridge, MA, 1961.
(26) Allison, S. A. *Macromolecules* **1996**, *29*, 7391–7401.
(27) Xin, Y.; Mitchell, H.; Cameron, H.; Allison, S. A. *J. Phys. Chem. B* **2006**, *110*, 1038–1045.
(28) Germann, M. W.; Turner, T.; Allison, S. A. *J. Phys. Chem. A* **2007**, *111*, 1452–1455.
(29) Hagerman, P.; Zimm, B. H. *Biopolymers* **1981**, *20*, 1481–1502.
(30) Pei, H.; Allison, S. A.; Haynes, B. M. H.; Augustin, D. *J. Phys. Chem. B* **2008**, *113*, 2564–2571.
(31) Schellman, J. A.; Harvey, S. C. *Biophys. Chem.* **1995**, *59*, 95–114.
(32) Tirado, M. M.; Martinez, C. L.; Garcia de la Torre, J. *J. Phys. Chem.* **1984**, *81*, 2047–2052.
(33) Eimer, W.; Williamson, J. R.; Boxer, S. G.; Pecora, R. *Biochemistry* **1990**, *29*, 799–811.
(34) Diaz, R.; Fujimoto, B. S.; Schurr, J. M. *Biophys. J.* **1997**, *72*, A322.
(35) Garcia de la Torre, J.; Bloomfield, V. A. *Biopolymers* **1977**, *16*, 1747–1763.
(36) Garcia de la Torre, J.; del Rio Echenique, J.; Ortega, A. *J. Phys. Chem. B* **2007**, *111*, 955–961.
(37) Allison, S. A.; Chen, C.; Stigter, D. *Biophys. J.* **2001**, *81*, 2558–2568.
(38) Lewis, R. J.; Allison, S. A.; Eden, D.; Pecora, R. *J. Chem. Phys.* **1988**, *89*, 2490–2503.
(39) Xin, Y.; Hess, R.; Ho, N.; Allison, S. A. *J. Phys. Chem. B* **2006**, *110*, 25033–25044.